



Accepted Article

Title: Engineering Low Volume Resuscitants for the Prehospital Care of Severe Hemorrhagic Shock

Authors: Trey J. Pichon, Xu Wang, Ethan E. Mickelson, Wen-Chia Huang, Shayna L. Hilburg, Sarah Stucky, Melissa Ling, Alexander E. St. John, Kristyn M. Ringgold, Jessica M. Snyder, Lilo D. Pozzo, Maggie Lu, Nathan J. White, and Suzie Pun

This manuscript has been accepted after peer review and appears as an Accepted Article online prior to editing, proofing, and formal publication of the final Version of Record (VoR). The VoR will be published online in Early View as soon as possible and may be different to this Accepted Article as a result of editing. Readers should obtain the VoR from the journal website shown below when it is published to ensure accuracy of information. The authors are responsible for the content of this Accepted Article.

To be cited as: Angew. Chem. Int. Ed. 2024, e202402078

Link to VoR: https://doi.org/10.1002/anie.202402078



RESEARCH ARTICLE

Engineering Low Volume Resuscitants for the Prehospital Care of Severe Hemorrhagic Shock

Trey J. Pichon, [a,b,c] Xu Wang, [c,d] Ethan E. Mickelson, [a,b,c] Wen-Chia Huang, [e] Shayna L. Hilburg, [b,f] Sarah Stucky, [c,d] Melissa Ling, [b,c] Alexander E. St. John, [c,d] Kristyn M. Ringgold, [c,d] Jessica M. Snyder, [g] Lilo D. Pozzo, [b,f] Maggie Lu, [e] Nathan J. White, * [b,c,d] Suzie H. Pun*[a,b,c]

[a] Trey J. Pichon, Ethan E. Mickelson, Suzie H. Pun Department of Bioengineering, University of Washington 3720 15th Ave NE, Seattle, Washington 98195, USA

E-mail: spun@uw.edu (SHP)

[b] Trey J. Pichon, Ethan E. Mickelson, Shayna L. Hilburg, Melissa Ling, Lilo D. Pozzo, Nathan J. White Molecular Engineering and Sciences Institute, University of Washington

3946 W Stevens Way NE, Seattle, Washington 98195, USA

[c] Trey J. Pichon, Xu Wang, Ethan E. Mickelson, Sarah Stucky, Melissa Ling, Alexander E. St John, Kristyn M. Ringgold, Nathan J. White, Suzie H. Pun Resuscitation Engineering Science Unit (RESCU)

University of Washington

Harborview Research and Training Building, Seattle, Washington 98104, USA

[d] Xu Wang, Sarah Stucky, Alexander E. St John, Kristyn M. Ringgold, Nathan J. White

Department of Emergency Medicine, University of Washington

Seattle, Washington 98195, USA

Email: whiten4@uw.edu (NJW)

[e] Wen-Chia Huang, Maggie Lu

Biomedical Technology and Device Research Laboratories

Industrial Technology Research Institute

Hsinchu, 300 Taiwan, Republic of China

[f] Shayna L. Hilburg, Lilo D. Pozzo

Department of Chemical Engineering, University of Washington

Seattle, Washington 98195, USA

[g] Jessica M. Snyder

Department of Comparative Medicine, University of Washington

Seattle, Washington 98195, USA

Supporting information for this article is given via a link at the end of the document.

Abstract: Globally, traumatic injury is a leading cause of suffering and death. The ability to curtail damage and ensure survival after major injury requires a time-sensitive response balancing organ perfusion, blood loss, and portability, underscoring the need for novel therapies for the prehospital environment. Currently, there are few options available for damage control resuscitation (DCR) of trauma victims. We hypothesize that synthetic polymers, which are tunable, portable, and stable under austere conditions, can be developed as effective injectable therapies for trauma medicine. In this work, we design injectable polymers for use as low volume resuscitants (LVRs). Using RAFT polymerization, we evaluate the effect of polymer size, architecture, and chemical composition upon both blood coagulation and resuscitation in a rat hemorrhagic shock model. Our therapy is evaluated against a clinically used colloid resuscitant, Hextend. We demonstrate that a radiant star poly(glycerol monomethacrylate) polymer did not interfere with coagulation while successfully correcting metabolic deficit and resuscitating animals from hemorrhagic shock to the desired mean arterial pressure range for DCR – correcting a 60% total blood volume (TBV) loss when given at only 10% TBV. This highly portable and non-coagulopathic resuscitant has profound potential for application in trauma medicine.

Introduction

Traumatic injuries account for a substantial portion of global morbidity and mortality and is the leading cause of death for persons aged 1-46 in the United States. [1] Among trauma-related fatalities, hemorrhagic shock from blood loss causes up to 40% of civilian deaths. Alarmingly, over half of these hemorrhagic deaths occur within the first minutes to hours after injury, often before patients can reach a hospital. [2,3] This critical timeframe underscores the urgent need for innovative strategies and therapies that can effectively address hemorrhage and achieve damage control resuscitation, even in the prehospital environment. The extensive blood loss from hemorrhage leads to

RESEARCH ARTICLE

hemorrhagic shock, a pathophysiologic state in which blood pressure collapses and the hypovolemic circulatory system is unable to adequately perfuse tissues or deliver oxygen. [4] The resulting hypoxia forces tissues into anaerobic respiration, thereby inducing lactic acidosis and the shutdown of cellular sodium pumps. The corresponding influx of sodium ions into cells is accompanied by a large volume of water that flows from the intravascular space and into the interstitium, exacerbating the hypovolemia and hemorrhagic shock. [5] Furthermore, the immune response that follows a traumatic injury generates high levels of inflammatory cytokines and reactive oxygen species. [6] This dysfunctional inflammatory response can cause severe secondary injury by ischemia reperfusion, which can lead to multiple organ failure and death. [7]

The goal of fluid resuscitation is to restore oxygen delivery to adequate levels to prevent progressive organ damage. However, aggressive fluid resuscitation in the setting of freely-bleeding wounds can disrupt clots and cause rebleeding events that worsen shock. Damage control resuscitation (DCR) is an approach that has been developed to maintain basal perfusion of vital organs without pushing blood pressures high enough to cause rebleeding.^[8] In past reports, we detail the development of a polymeric hemostat, PolySTAT, to address the threat of rebleeding during treatment of hemorrhagic shock. [9-12] In this work, we focus on developing potent polymeric resuscitants designed for DCR in emergency and prehospital environments. The current standard of care resuscitants, crystalloid and colloid solutions, operate on the principle of aggressive fluid replacement. These approaches require several liters of treatment that must be warmed to physiological temperature before use, rendering these large volume resuscitants impractical in prehospital settings.[13-15] The large volumes administered to trauma patients dilute coagulation factors, spike blood pressure, and encourage tissue edema.[15-17] In austere prehospital environments, such as air evacuations and military settings, it is particularly advantageous for resuscitation fluids to be lowervolume and lighter-weight. Modern resuscitation strategies in accordance with DCR intentionally limit fluid administration and instead rely upon whole blood transfusions, thereby reducing coagulopathy, inflammation, and mortality.[18,19] However, logistical challenges prevent regular use of blood products in the prehospital setting, particularly as they are of extremely limited supply.

Alternative approaches in development include synthetic low volume resuscitants (LVRs) having unique and favorable properties. Polyethylene glycol of molecular weight 20kDa (PEG20K) is currently a lead candidate for LVR and operates as a hybrid cell impermeant and oncotic agent. The cell impermeant component of PEG20K allows it to partially extravasate from the vasculature and pull fluid directly out of interstitial cells, while the oncotic component remains in the bloodstream to further draw fluid into the vascular space (SI Figure 1). These polymers achieve resuscitation by generating oncotic pressure gradients, which relocate fluid from the interstitium into the patient's vasculature, essentially using the patient's own interstitial fluid

reserve for resuscitation. PEG20K has demonstrated a potency 12-18x greater than crystalloid/colloid solutions, shrinking the volume of therapy needed for resuscitation and comprising a therapy that is exponentially more portable and conducive to prehospital applications.F^[20]

Despite promising preclinical results in animal models, PEG20K impairs coagulation, inducing a state of platelet passivation similar to thrombocytopenia.[21] Other concerns arise from the increased prevalence of PEG-induced anaphylaxis and other allergic reactions, which rose correspondingly with PEGcontaining COVID-19 vaccines. [22,23] In this work, we leverage our lab's experience with methacrylate-based polymers and the polymerization technique, Reversible Addition Fragmentation chain Transfer polymerization (RAFT), to create a highly tunable polymer platform for the rational design of LVRs. The chemical flexibility and side-chain tailorability of methacrylates enabled us to easily vary polymer architecture, radius of gyration, and monomer compositions to reveal how polymer properties influence resuscitative profile, coagulopathic effects, and circulation time. Herein, we report the design and synthesis of LVRs that provide effective resuscitation in rat trauma models without disrupting coagulation.

Results and Discussion

Synthesis and characterization of linear neutral and zwitterionic hydrophilic polymers for low volume resuscitation

To begin with, we explored different size ranges of methacrylate-based resuscitants to observe the influence on resuscitation. We completed some simple theoretical calculations of polymer contour length, average square end-to-end distance, and $R_{\rm g}$ as outlined in the supplementary information, and found a methacrylate with a degree of polymerization (DP) of 125 would theoretically give us an $R_{\rm g}$ approximately half that of PEG20K. We therefore selected a panel of poly(glycerol monomethacrylate) (pGmMA) linear homopolymers with DPs of 100, 200, and 300. The oncotic potential of these neutral pGmMA LVRs should be closely related to the osmotic pressure (\Pi) of the polymers in solution which is proportional to their molar concentration, as dictated by van't Hoff's equation:

$$\Pi = \frac{n_{solute}RT}{V}$$

Where n_{solute} = the number of moles of polymer in solution, V = volume, R = molar gas constant, and T = temperature. Interestingly, highly charged macromolecules such as albumin exhibit a larger osmotic pressure than predicted by van't Hoff's equation due to the Gibbs-Donan effect. [24] We hypothesized highly-charged zwitterionic monomers would increase the oncotic potential of our LVRs, enabling us to use a lower polymer dose. We selected 2-methacryloyloxyethyl phosphorylcholine (MPC) and N-(3-sulfopropyl)-N-methacroyloxyethyl-N,N-dimethylammonium betaine (SBMA) to evaluate alongside

RESEARCH ARTICLE

GmMA. Both monomers exhibit over double the number of coordinated water molecules compared to GmMA, as determined by differential scanning calorimetry (DSC). [25] Based on the logic above, we synthesized a panel of linear polymers of DP100, 200, and 300 using the three monomers (L-GmMA, L-MPC, and L-

SBMA) via RAFT polymerization (SI Reaction Scheme 1) as shown in Figures 1A-C. Polymers were synthesized with molecular weights (Mn) of approximately 18 kDa to 90 kDa and with narrow polydispersity indices (PDIs) (1.02-1.25) (Figure 1D-F, SI Table 1, SI Figures 2-4).

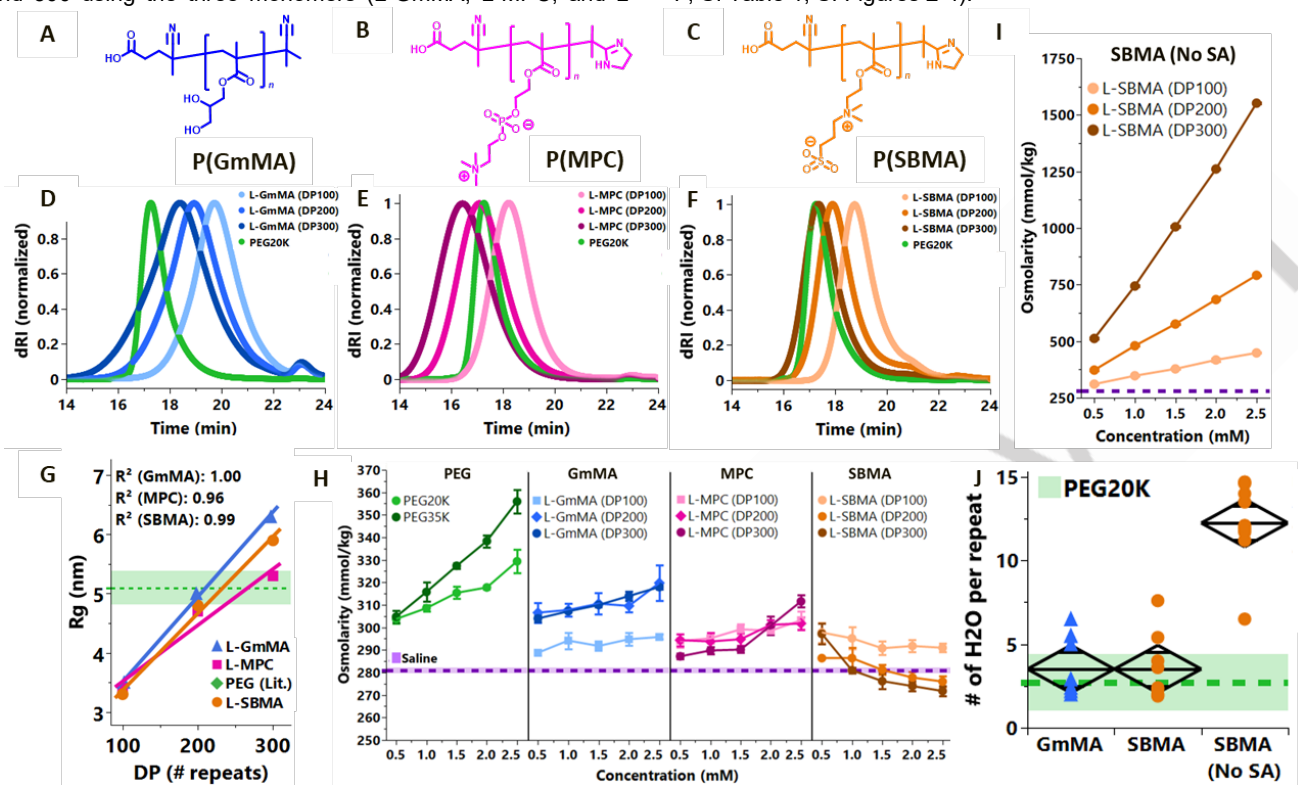


Figure 1. Characterization of linear LVRs synthesized via RAFT. A-C) Molecular structure of L-GmMA, L-MPC, and L-SBMA, respectively. D-F) Gel Permeation Chromatograms of DP100, 200, and 300 L-GmMA, L-MPC, and L-SBMA LVRs, respectively. Each trace is overlaid with PEG20K (green) as a comparison. The Mn and PDI were determined using 100% mass recovery (RI Detector, Wyatt Optilab T-rex) and multiangle light scattering (MALS, Wyatt miniDAWN Treos) gel permeation chromatography (GPC). The running solvent was phosphate buffered saline (PBS) (flow rate: 0.5 mL/min) at room temperature and samples were prepared at 10 mg/mL. G) Small-angle x-ray scattering (SAXS) radius of gyration measurements as a function of degree of polymerization. The green dotted line with ± 1 SEM interval band represents the size range of PEG20K measured in literature.^[26] The DP200 L-GmMA (blue line, MW = 32 kDa), L-MPC (magenta line, MW = 59 kDa), and L-SBMA (orange line, MW = 56 kDa) all have a similar R_g compared to PEG20K (MW = 20 kDa). All polymers were evaluated at 5 mg/mL and 15 mg/mL in PBS (pH 7.4). Data shown are from monodisperse gaussian coil model fits from scattering data for 15 mg/mL. Fit data confirmed that there is no effect due to concentration between the 5 mg/mL and 15 mg/mL samples. H) Vapor pressure osmometry measurements of PEG20K and 35K (green/left), L-GmMA (blue/middle left), L-MPC (magenta/middle right), and L-SBMA (orange/right). All polymers were dissolved in normal saline. The purple line shows the osmolarity of the normal saline for reference. All measurements were done using a Vapro 5600 in triplicate. Error bars are 1 standard deviation from the mean. I) Vapor pressure osmometry measurements of L-SBMA (orange) with no self-assembly (No SA). All polymers were dissolved in normal saline with additional NaCl to match the number of moles of repeat units. The purple line shows the osmolarity of the normal saline only. All measurements were done using a Vapro 5600 in triplicate. Error bars are 1 standard deviatio

We characterized the polymer panel using small-angle x-ray scattering (SAXS) to measure radii of gyration (Rg) (Figure 1G and SI Figure 5). The DP200 L-GmMA (MW = 32 kDa), L-MPC (MW = 59 kDa), and L-SBMA (MW = 56 kDa) all have similar Rg as PEG20K, as expected from our theoretical calculations. Next, we measured the osmolarity of the linear polymer panel in normal saline (0.9% w/v NaCl, isotonic to blood serum) by vapor pressure osmometry (Figure 1H). DP200 and DP300 L-GmMA showed similar osmolarity to PEG20K while L-MPC and L-SBMA showed lower osmolarity compared to PEG20K. In the case of L-SBMA, there was a decrease in osmolarity as the molar concentration

increased. There are likely two factors contributing to the phenomenon. First, pSBMA can self-assemble as a function of concentration in solutions with low ionic strength, which would create larger macromolecules that decrease the overall number of moles of solute in solution. Second, as polymer concentration is increased, pSBMA may be coordinating salt ions from the normal saline solution. The drop in osmolarity below the 0.9% NaCl solution level (purple line in Figure 1G) at high polymer concentrations supports this hypothesis. The apparent drop in osmolarity as polymer concentration is increased is an artifact of the experimental set-up; there are a fixed number of ions in

RESEARCH ARTICLE

solution during osmometry measurements, whereas in the body there would be large reserves outside the vascular space to compensate for the zwitterions. With this detail in mind, we repeated the L-SBMA osmometry measurements (Figure 1I) but included additional NaCl to match the molar concentration of the zwitterionic groups and prevent self-assembly. We observed ~2-6x increase in the osmolarity of pSBMA. With L-MPC, we have not seen any evidence of self-assembly in our work, nor have we seen self-assembly documented in literature. Finally, we measured the hydration number (n_H) or the number of strongly bound, non-freezing water molecules coordinated per repeat unit using DSC for PEG20K, L-GmMA, and L-SBMA (Figure 1J, SI Table 1). In 0.9% NaCl solution, L-GmMA and L-SBMA had similar n_H values to PEG20K. However, in agreement with the osmometry measurements for L-SBMA, when additional NaCl was added to coordinate with the zwitterionic groups to prevent self-assembly, we observed a ~4x increase in the amount of water coordinated per polymer repeat.

Linear LVRs underperform in rotational thromboelastometry evaluation and a severe hemorrhagic shock model in rats.

We next employed rotational thromboelastometry (ROTEM) to evaluate the effect of the linear LVRs on coagulation using human plasma. ROTEM monitors clot firmness over time, characterizing clot formation and breakdown (Figure 2A). For our analysis, we kept molar concentrations of polymers constant by analyzing 10%, 20%, and 30% w/v solutions of DP100, 200, and 300 polymers, respectively, at 10% total plasma volume in ROTEM.^[27,28] The various linear LVRs were evaluated against a normal saline volume control for their clotting times (SI Figure 6), alpha angle (Figure 2B), and maximum clot firmness (MCF) (Figure 2C).

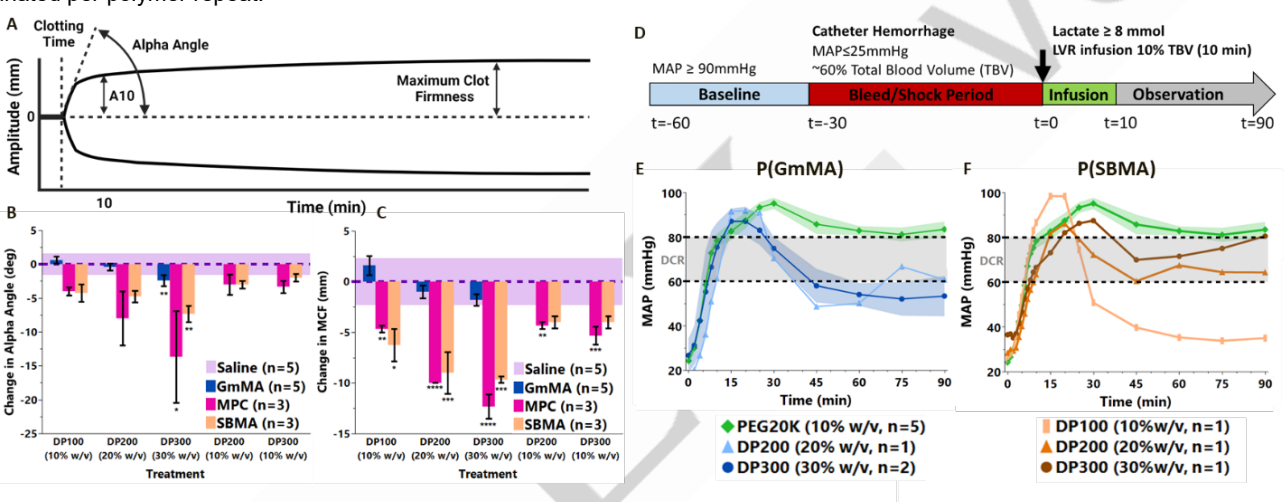


Figure 2. In vitro (A-C) and in vivo (D-F) Screening of Linear LVRs. A) General schematic of the key ROTEM parameters. Alpha angle is a measure of clot formation kinetics, while MCF is a measure of the firmness of the clot. B) Change in alpha angle measured in degrees for human plasma treated with 10% of total blood volume (TBV) of pGmMA (dark blue), pMPC (magenta), and pSBMA (light orange). C) Change in MCF measured in mm for human plasma treated with 10% of TBV of pGmMA (blue), pMPC (magenta), and pSBMA (orange). For all EXTEMs, the data displayed is the difference from a normal saline volume control run at the same time for each donor. A purple dotted line with a ± 1 SEM (standard error of measurement) band is placed at zero to represent the normal saline control. A fit model for a repeated measure, one-way ANOVA with Tukey post-hoc analysis (α = 0.050) with donor as a random source effect was used. All error bars and bands represent ± 1 SEM from the mean. For all the ROTEM data, significance labels were used to indicate if there is a statistically significant difference when comparing the polymers to the normal saline volume control. The following significance labels were used: ns (P > 0.05), * $(P \le 0.05)$, *** $(P \le 0.01)$, **** $(P \le 0.001)$, **** $(P \le 0.001)$, **** 0.0001). D) Overview of the severe hemorrhagic shock model in rats. E) Screening study to observe the ability of DP200 and DP300 L-GmMA to rescue and maintain blood pressure in the target MAP range (grey band). Comparison of the mean arterial pressure (MAP) in mmHg during the infusion and observation time of the study for rats treated with pGmMA, DP200 (20% w/v, n=1, light blue triangles) and DP300 (30% w/v, n=2, dark blue circles). F) Screening study to observe the ability of DP100, DP200, and DP300 L-SBMA to rescue and maintain blood pressure in the target MAP range (grey band). Comparison of the MAP in mmHg during the infusion and observation time of the study for rats treated with pSBMA of DP100 (10% w/v, n=1, light orange rectangles), DP200 (20% w/v, n=1, orange triangles) and DP300 (30% w/v, n=1, dark orange circles). All rats were given an estimated 10% TBV dose of LVR therapy. PEG20K (10% w/v, n=5, green diamonds) was used as a positive control. The target range for MAP in damage control resuscitation of ~60-80 mmHg is shown by a grey band. All error bars and bands represent ± 1 SEM from the mean. Due to the low sample size, no statistics were run on the data.

L-GmMA minimally affected coagulation, with only the DP300 showing a significant change in alpha angle. In contrast, both L-MPC and L-SBMA induced hypocoagulability in the plasma of human donors, decreasing both the rate of clot formation and the overall clot firmness in ROTEM, significantly impairing coagulation. Since MCF correlates highly with plasma fibrinogen

levels, the decrease in clot firmness could suggest that the zwitterions are either inhibiting the activation of fibrinogen into fibrin, or that the zwitterions are disrupting fibrin polymerization and changing clot structure, resulting in softer clots.^[29]

RESEARCH ARTICLE

Next, we evaluated L-GmMA and L-SBMA polymers in vivo using a lethal and severe rat hemorrhagic shock model (Figure 2D). Blood pressure as a function of time is shown for DP200 and 300 L-GmMA (Figure 2E) and DP100, 200, and 300 L-SBMA (Figure 2F). The target range for mean arterial pressure (MAP) in damage control resuscitation is ~60-80 mmHg, which balances reperfusion of tissues with hypotension to prevent rebleeding and coagulopathy.[30] From the initial in vivo pilot experiment, DP300 L-GmMA (n=2) temporarily reaches the desired MAP range, but subsequently drops below the range. DP300 L-SBMA of (n=1) maintains MAP within the target range throughout the evaluation. These initial studies indicated that for L-GmMA, we needed to prevent premature clearance and increase oncotic potency; for L-SBMA, we needed to prevent coagulopathies. We hypothesized that restructuring our linear polymers into a radiant star architecture would increase oncotic potency by increasing the surface area available for interactions with water, leading to a higher density of coordinated water molecules. Similarly, it has been shown that hyper-branched PEG (HPG) has a higher density of coordinated water compared to linear PEG. HPG also exhibited better blood compatibility compared to its linear counterparts of similar molecular weights. [31–33] Additionally, HPG and cyclic polymers have improved biodistribution compared to their linear counterparts of similar molecular weight due to a decreased ability to reptate through nanopores such as the fenestrated glomerular endothelium in the kidney. [32,34] Similarly, we hoped that moving to a radiant star architecture would impede this reptation and therefore reduce renal excretion rates.

Synthesis and characterization of radiant star neutral and zwitterionic hydrophilic polymers for low volume resuscitation

Figure 3A below outlines the synthesis of radiant star polymers using RAFT polymerization adapted from Das *et al.*^[35] Further details are available in the SI Reaction Scheme 2. Because L-MPC polymers seemed to impact coagulation slightly more compared to L-SBMA in ROTEM experiments, we focused only on radiant star versions of pGmMA (RS-GmMA) and pSBMA (RS-SBMA).

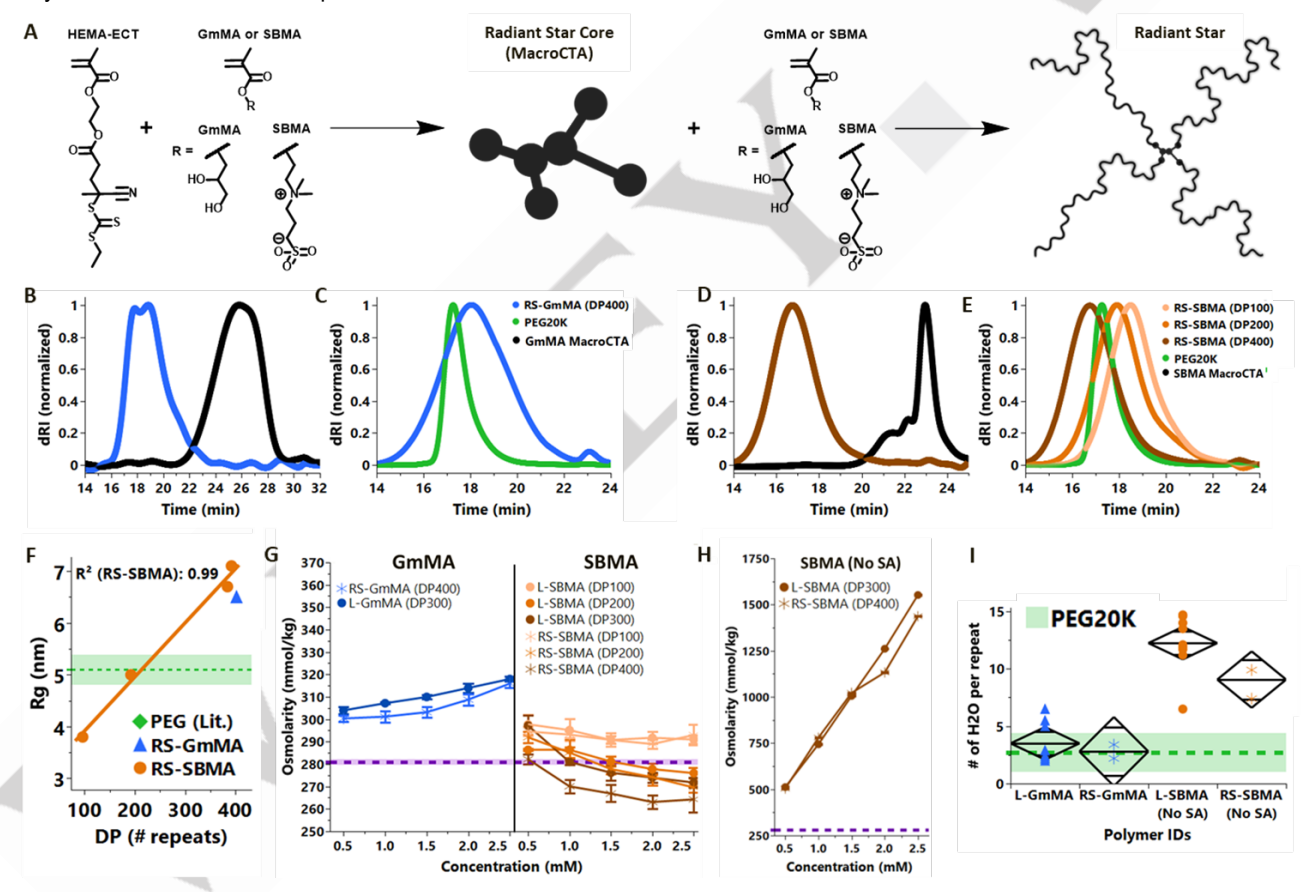


Figure 3. Characterization of Radiant Star LVRs synthesized via RAFT Polymerization. A) Reaction scheme for copolymerization of either GmMA or SBMA with HEMA-ECT (hECT) to create macro-chain transfer agents (macroCTAs) for the radiant star cores. This is followed by chain extension with either GmMA or SBMA to create radiant star LVRs (RS-GmMA and RS-SBMA, respectively). B) GPC showing successful chain extension of the GmMA macroCTA core (black) to prepare DP400 RS-GmMA (blue). C) GPC trace of DP400 RS-GmMA radiant star (blue) D) GPC showing successful chain extension of SBMA macroCTA core (black) to prepare DP400 RS-SBMA (dark orange). E) GPC traces of DP100 (light orange), 200 (orange), and 400 RS-SBMA (dark orange), respectively. For all GPCs PEG20K (green) is overlaid for comparison. The molecular weight (Mn) and polydispersity index (PDI) were determined using 100% mass recovery (RI Detector, Wyatt Optilab T-rex) and multiangle light scattering (MALS, Wyatt miniDAWN Treos) gel permeation chromatography (GPC). The running solvent for both RS-GmMA and its macroCTA was DMF with 1g/L of LiBr flow rate: 0.8 mL/min) at 60°C withsamples prepared at 10 mg/mL. The running solvent for the RS-SBMA and their macroCTA was phosphate buffered saline (PBS) (flow rate: 0.5 mL/min) at room temperature with samples prepared at 10 mg/mL. F) Small-angle x-ray

RESEARCH ARTICLE

scattering (SAXS) radius of gyration (R_9) measurements as a function of DP. The green dotted line with \pm 1 SEM interval band represents the size range of PEG20K measured in literature. [28] DP400 RS-GmMA (blue triangle, MW = 70 kDa), DP400 RS-SBMA (orange circles, MW = 118 kDa), all have larger R_9 compared to PEG20K (MW = 20 kDa). All polymers were evaluated at 5 mg/mL and 15 mg/mL in PBS (pH 7.4). Data shown are from fits to star polymer models from scattering data for 15 mg/mL. Fit data confirmed that there is no effect due to concentration between the 5 mg/mL and 15 mg/mL samples. G) Vapor pressure osmometry measurements of pGmMA (blue/middle) and pSBMA (orange/right). Linear LVRs (circles) are shown for reference to radiant stars (asterisks). All polymers were dissolved in normal saline. The purple line (\pm 1 standard deviation) shows the osmolarity of the normal saline for reference. All measurements were done using a Vapro 5600 in triplicate. Error bars are \pm 1 standard deviation from the mean. H) Vapor pressure osmometry measurements of DP400 RS-SBMA (orange asterisks) compared to DP300 L-SBMA (orange circles) with no self-assembly (No SA). All polymers were dissolved in normal saline with additional NaCl added to match the number of moles of repeat units. The purple line shows the osmolarity of the normal saline for reference. All measurements were done using a Vapro 5600 in triplicate. Error bars are 1 standard deviation from the mean. I) DSC measurements of the $n_{\rm H}$ for L-GmMA (blue triangle/left) compared to RS-GmMA (blue asterisk/2nd left), and L-SBMA (orange/2nd right) compared to RS-SBMA (orange asterisk/right) without self-assembly (No SA). A green dotted line with \pm 1 SEM interval band represents the $n_{\rm H}$ of PEG20K controls. All polymers were dissolved in normal saline. To prevent self-assembly, additional NaCl was added to match the number of moles of repeat units.

We synthesized RS-SBMA of DP100 and DP200 to directly compare to their linear counterparts. We hypothesized that higher molecular weight radiant star polymers would improve in vivo performance, and therefore synthesized DP400 RS-SBMA and RS-GmMA polymers. Figure 3B-E shows the GPC traces of the final synthesized radiant stars, confirming successful chain extension of the macroCTAs. We synthesized a range of RS-SBMA and RS-GmMA polymers with a comparable range of PDIs (1.02-1.12) and molecular weights (~ 35 kDa to 118 kDa) to their linear counterparts (SI Figures 7-11 and SI Table 2). The molecular weights of our macroCTAs (GmMA = 5.7 kDa, SBMA = 7.1 kDa) from GPC were comparable to those reported by Das et al.[35] From the conversion of both the HEMA-ECT and its comonomer (either GmMA or SBMA) in ¹H NMR analysis, we calculated the radiant stars have an average of ~3.6 arms. This agreed with SAXS analysis, which indicated that approximately 3 arms provided the best fit of the data (SI Table 3 and SI Figure 12). From SAXS analysis (Figure 3F), we found that the DP100 and DP200 RS-SBMA had similar Rq to their linear counterparts, while DP400 RS-GmMA and RS-SBMA had R_q ~1 nm larger compared to the DP300 linear polymers. We conducted a small in vivo study (n=3 per treatment) to compare the biodistribution of DP300 L-GmMA to DP400 RS-GmMA during the severe hemorrhagic shock model in rats. The RS-GmMA and L-GmMA showed a similar mass-to-volume plasma concentrations (mg/mL) across all time points (SI Figure 13) despite the L-GmMA being given at a 1.5x higher (30% w/v) infusion compared to the RS-GmMA (20% w/v). This would suggest that the L-GmMA is rapidly cleared from the bloodstream, resulting in a lower than expected plasma concentration. The percentage of injected dose in the plasma at T90 (SI Figure 14) for RS-GmMA was significantly higher (p = 0.0005) compared to L-GmMA (~27% vs. ~15%, respectively). Although not statistically significant, there was a trend towards L-GmMA having a higher percentage of the injected dose at T90 in the kidneys and urine compared to RS-GmMA. Overall, the DP400 RS-GmMA was retained in plasma better than DP300 L-GmMA. However it is still unknown if this improvement was due to the larger $R_{\mbox{\scriptsize g}}$ or the radiant star architecture. Next, we ran vapor pressure osmometry on the radiant stars and observed similar osmolarity trends as their linear counterparts, including the decrease in osmolarity with molar concentration in normal saline for RS-SBMA (Figure 3G). Again, additional NaCl prevented the self-assembly and resulted in a higher osmolarity (Figure 3H). The DSC measurements of n_H again mirrored the trend seen in osmometry (Figure 3I and SI Table 2). The DP400 RS-GmMA and RS-SBMA coordinated a similar number of non-freezing water molecules to their linear versions. Using R_{q} data from SAXS and n_{H} data from DSC, we calculate that DP400 RS-SBMA has a density of ~2.4 H2O per nm³, whereas the L-SBMA of DP100, DP200, and DP300 have water densities of ~7.8, 5.1, and 4.6 H₂O per nm³, respectively, suggesting that the density of coordinated water is lower for the radiant star architecture compared to linear architecture. DP400 RS-GmMA has a density of ~1 H₂O per nm³, whereas L-GmMA of DP100, DP200, and DP300 have water densities of ~1.5, 1.8, and 0.9 H₂O per nm³, respectively (SI Tables 1 and 2). The number of arms extending from the radiant star core may need to be increased to see the benefits observed with HPG.[36]

RS-GmMA is the first resuscitant to ever demonstrate no adverse effects upon coagulation

Based on preliminary *in vivo* dosing experiments, we selected a 20% w/v solution of RS-GmMA (DP400) and RS-SBMA (DP400) in order to match concentrations between coagulation assays and *in vivo* studies (SI Figure 15). We found that in whole blood, (Figure 4A-B below and SI Figure 16), PEG20K and RS-SBMA both increased clotting time compared to normal saline, while Hextend, PEG20K, and RS-SBMA all decrease clotting kinetics and lead to overall softer clots (Figure 4A-B below and SI Figure 16). PEG20K and RS-SBMA were not statistically different from each other, and both impacted clotting similarly, leading to a hypocoagulable state with decreased clot firmness. The RS-GmMA did not show a statistical difference from normal saline across the typical ROTEM parameters reported and was therefore the only material that did not adversely affect coagulation.

RESEARCH ARTICLE

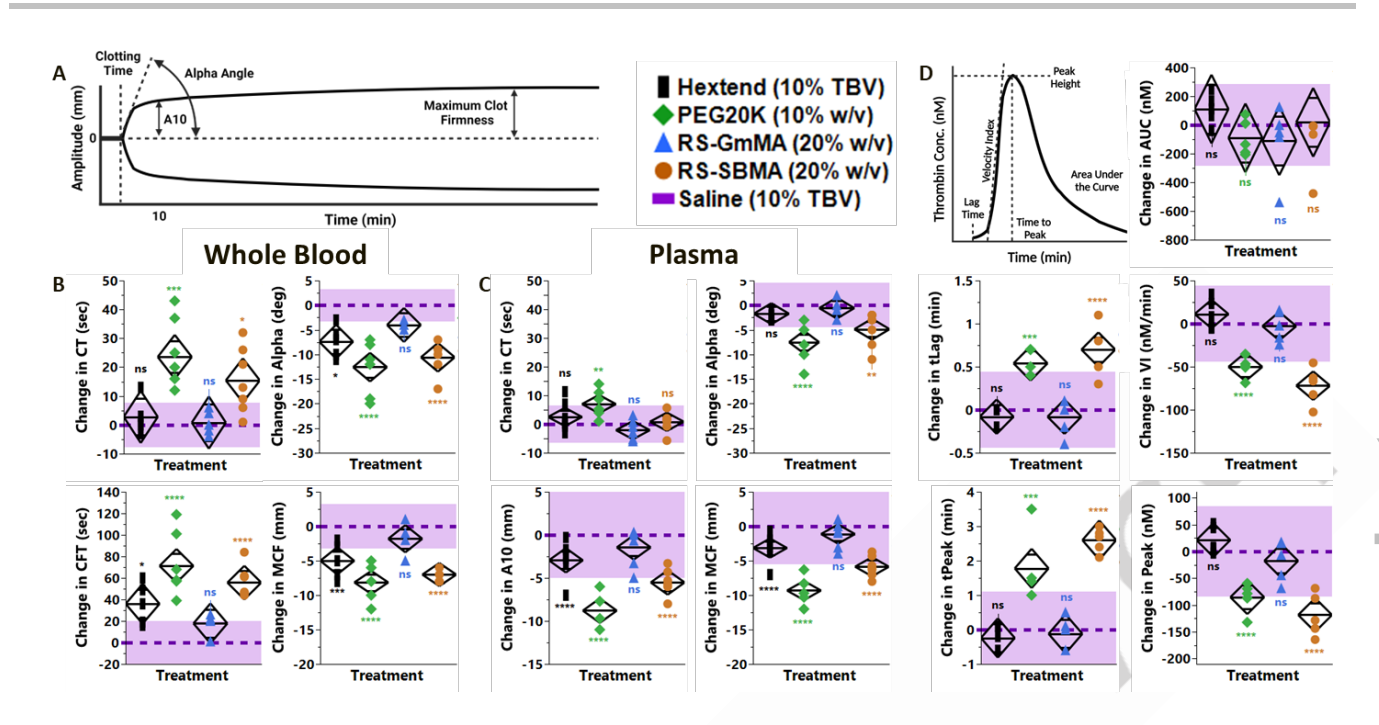


Figure 4. Characterization of Radiant Star LVRs synthesized via RAFT Polymerization. In vitro characterization of the effect of Radiant Star LVRs on coagulation in comparison to PEG20K and Hextend. For all clotting assays, Hextend (clinical standard colloid control), RS-GmMA (20% w/v), RS-SBMA (20% w/v), PEG20K (10% w/v), and normal saline were all evaluated at 10% TBV. All treatments were dissolved in veterinarian-grade 0.9% normal saline. A) General schematic of key ROTEM parameters. Clotting time (CT) is the time it takes for clots to begin forming, Alpha Angle is a measure of clot formation kinetics, while A10 and Maximum Clot Firmness (MCF) are measures of clot firmness at ten minutes and the maximum overall during the clotting time period (60 minutes), respectively. B) ROTEM evaluation of final LVRs in human whole blood (n = 5-7). Top left: Change in clotting time measured in seconds. Top right: Change in alpha angle measured in degrees. Bottom left: Change in clot firmness time measured in seconds. Bottom right: Change in maximum clot firmness (MCF) measured in mm. A fit model for a repeated measure, one-way ANOVA with Tukey post-hoc analysis (a = 0.050) with donor as a random source effect was used. C) ROTEM evaluation of final LVRs in human plasma (n = 7). Top left: Change in clotting time measured in seconds. Top right: Change in alpha angle measured in degrees. Bottom left: Change in A10 measured in mm. Bottom right: Change in MCF measured in mm. For both whole blood and plasma, the data displayed is the difference from a normal saline volume control run at the same time for each donor. A purple dotted line with the 95% confidence interval band is placed at zero to represent the normal saline control. A fit model for a repeated measure, one-way ANOVA with Tukey post-hoc analysis (q = 0.050) with donor as a random source effect was used. All diamonds and bands represent the 95% confidence interval. D) Top left: overview of thrombin generation assay (TGA) metrics measured in human plasma. Lag time (tLag) is the time it takes for thrombin to begin being generated, Velocity Index (VI) is the rate of thrombin generation, Time to Peak (tPeak) is how long it takes to reach the maximum thrombin concentration, Peak Height (Peak) is the maximum concentration of thrombin measured, and Area Under the Curve (AUC) is the total amount of thrombin generated during coagulation; n =5 donors were evaluated. Top right: Change in the area under the TGA curve measured in nM. Middle left: Change in tLag measured in minutes. Middle right: Change in VI or the slope of the initiation phase measured in nM/min. Bottom left: Change in tPeak measured in minutes. Bottom right: Change in the peak thrombin concentration measured in nM. The data displayed is the difference from a normal saline volume control run at the same time for each donor. A purple dotted line with the 95% confidence interval band is placed at zero to represent the normal saline control. A fit model for a repeated measure, one-way ANOVA with Tukey post-hoc analysis (α = 0.050) with donor as a random source effect was used. All diamonds and bands represent the 95% confidence interval. For all data, significance labels were used to indicate if there is a statistically significant difference when comparing the polymers to the normal saline volume control. The following significance labels were used: ns (P > 0.05), * (P \leq 0.05), ** (P \leq 0.01), **** (P \leq 0.001), **** (P \leq 0.001).

Next, we evaluated the same treatments in human plasma to remove platelets and evaluate the treatment effect on fibrinogen (Figure 4C and SI Figure 17). Similar to whole blood, we found that PEG20K increased the clotting time of human plasma, and that Hextend, PEG20K, and RS-SBMA all led to a significant decrease in clot firmness resulting in a hypocoagulable state. To evaluate whether Hextend, PEG20K, and RS-SBMA disrupt thrombin activity, we investigated the effect of the treatments on thrombin generation in human plasma by thrombin generation assay (TGA) (Figure 4D and SI Figure 18). We observed that PEG20K and RS-SBMA decrease the peak thrombin concentration (tPeak) and shift the thrombin generation curve down to later time points by increasing the lag phase (tLag) and

decreasing the rate of thrombin generation (VI). However, the total amount of thrombin generated, quantified from the AUC, stays the same across treatments. Thrombin concentration affects fibrin fibril structure, suggesting that PEG20K and RS-SBMA are delaying the conversion of prothrombin into thrombin, but not fully disrupting it, leading to softer clots.^[37] Knowing that Hextend does not affect thrombin but still demonstrates significant coagulopathy, we conclude that Hextend is most likely directly acting on fibrin and fibrinogen to impair clot formation.

We then evaluated the effect of the radiant stars and PEG20K upon platelet activation (SI Figure 19) and aggregation (SI Figure 20) to probe any ramification on primary hemostasis with

RESEARCH ARTICLE

treatment. When compared to the volume negative controls, there was no statistically significant change in platelet activation or aggregation, indicating that PEG20K, RS-GmMA, and RS-SBMA do not cause platelet dysfunction. From ROTEM, we can estimate the platelet contribution to MCF by subtracting the MCF in plasma from the MCF measured in whole blood (SI Figure 21). Once again, we did not observe a statistically significant effect on platelets for any of the treatments. In summary, the *in vitro* coagulation assays indicate that PEG20K, RS-SBMA, and

Hextend can induce a hypocoagulable state in human blood, but that RS-GmMA does not adversely affect coagulation.

Radiant star GmMA and SBMA correct severe hemorrhagic shock in rats to the desired blood pressure range for damage control resuscitation

We proceeded to evaluate Hextend, PEG20K, RS-SBMA (DP400), and RS-GmMA (DP400) in a severe hemorrhagic shock rat model. Figure 5A below shows an overview of the model.

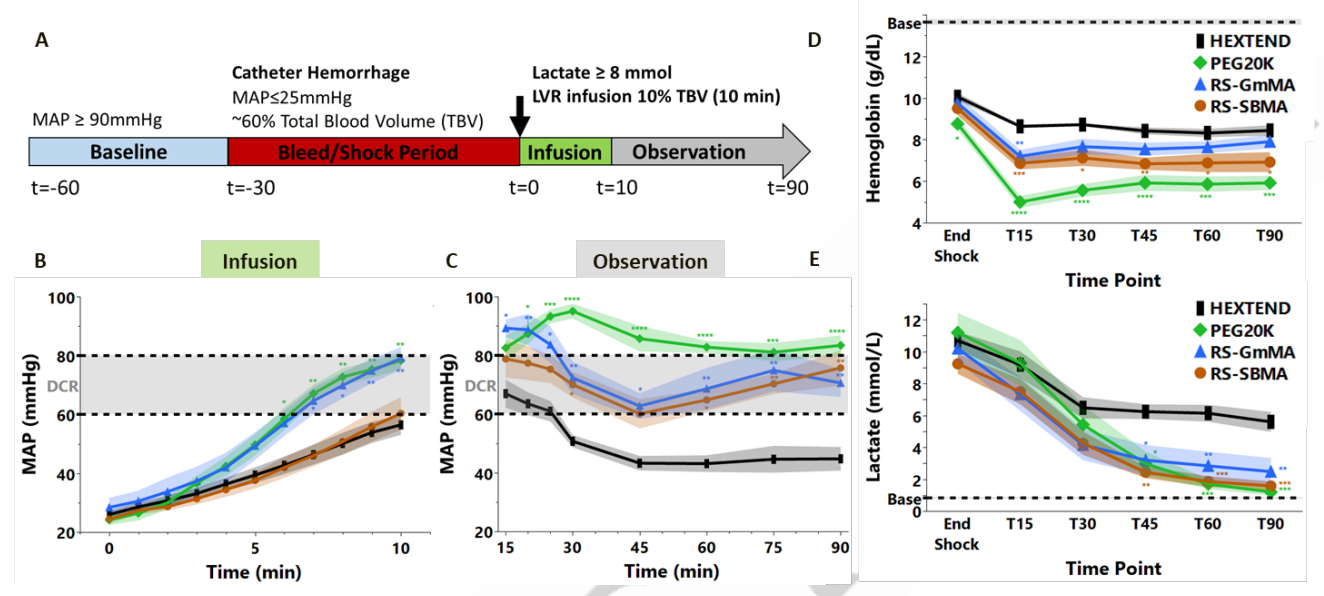


Figure 5. In vivo evaluation of Radiant Star LVRs in severe hemorrhagic shock model in rats (n=5) in comparison to PEG20K and Hextend. A) Overview of the severe hemorrhagic shock model in rats. Hextend (black rectangles, 6% w/v), PEG20K (green diamonds, 10% w/v), RS-GmMA (blue triangles, 20% w/v), and RS-SBMA (orange circles, 20% w/v) were all given at 10% TBV. Hextend was given in its standard commercial formulation, while PEG20K and the radiant stars were dissolved in 0.9% veterinarian-grade normal saline. B) Comparison of the mean arterial pressure (MAP) in mmHg during the infusion period (t=10 minutes) for rats. C) Comparison of the MAP in mmHg during the observation period for rats. D) Lactate concentration (mM) at various time points during the study. E) Hemoglobin (Hb) concentration (g/dL) at various time points during the study. For all plots, a black dotted line with the \pm 1 SEM interval band is placed at zero to represent the baseline levels for the rats. All error bands represent \pm 1 SEM. The target range for MAP in damage control resuscitation of ~60-80 mmHg is shown by a grey band. A fit model for a repeated measure, one-way ANOVA with Tukey post-hoc analysis (α = 0.050) was used for statistical analysis. For all data, significance labels were used to indicate if there is a statistically significant difference when comparing the LVRs (PEG20K, RS-GmMA, and RS-SBMA) to Hextend at each timepoint. The following significance labels were used: ns (P > 0.05), *(P \leq 0.05), **(P \leq 0.01), **** (P \leq 0.001).

All rats had a similar average percentage of TBV removed during the catheter hemorrhage period, ~58%, ~60%, ~57%, and ~59% for Hextend, PEG20K, RS-SBMA, and RS-GmMA, respectively. After reaching blood lactate ≥ 8 mmol/L (typically 30-45 minutes of shock), the rats were given a single bolus infusion of treatment over ten minutes. All treatments were administered at an estimated 10% of TBV for the rat. Figure 5B and SI Figures 22-23 show the change in blood pressure, heart rate, and the diastolic shock index (DSI) during the infusion and observation periods for each of the treatments. Interestingly, during the infusion the RS-SBMA showed a similar rate of increase in blood pressure to Hextend, whereas the RS-GmMA performed similarly to PEG20K, reflecting the osmolarity and DSC measurements of RS-SBMA. During administration, RS-SBMA is likely self-assembled at its reconstitution concentration of 20% w/v, as it becomes diluted in the bloodstream of the rat, it disassembles, leading to a slower onset of oncotic response.

All treatments show an initial peak of blood pressure between 15 and 30 minutes after administration, followed by a drop in blood pressure likely due to renal clearance. At 75 min and 90 min, there is no statistical difference between PEG20K, RS-GmMA, and RS-SBMA, whereas Hextend is significantly lower than the other three treatments (Figure 5C). Figure 5D-E and SI Figures 24-27 show blood gas results from the study which indicate how well the metabolic dysfunction of hemorrhagic shock is being corrected. RS-GmMA, RS-SBMA, and PEG20K all similarly decreased lactate levels, while Hextend did not reduce lactate levels. The hemoglobin concentration reflects the amount of water drawn into the bloodstream by the resuscitants, as hemoglobin (Hb) is diluted as the vascular space is refilled with interstitial water during resuscitation. We found that both RS-SBMA and PEG20K both had statistically significant lower Hb levels, while RS-GmMA was similar to Hextend. The lower osmolarity and n_H of RS-GmMA compared to RS-SBMA may have decreased the amount of water drawn in the bloodstream, allowing Hb levels to remain higher. We also found that both PEG20K and RS-GmMA returned ion

RESEARCH ARTICLE

concentrations to near-baseline levels (SI Figure 23). Recall that hemorrhagic shock shuts down cellular ion pumps,[38] increasing potassium levels while decreasing sodium levels in the blood. Although rats treated with RS-SBMA showed similar blood pressure, hemoglobin, and lactate levels to PEG20K, their potassium and sodium levels were significantly elevated at 60 and 90 min. We hypothesize that RS-SBMA is coordinating these ions retaining them in the blood. Finally, the kidneys, liver, heart, and lungs of the rats were submitted for histopathologic analysis by a board-certified veterinary pathologist. Histologic lesions were generally minimal to mild when observed, and no significant differences were identified between the treatment groups (SI Figure 28). In summary, the in vivo blood pressure and hemoglobin levels indicate that PEG20K, RS-GmMA, and RS-SBMA show similar ability to refill the vascular space, while lactate levels support a similar ability to correct the metabolic deficit created by hemorrhagic shock. Even with the high polymer doses no adverse effects were observed in hemodynamics or in histopathology of major organs.

Conclusion

In this study, methacrylates of various sizes, chemistries, and architectures were evaluated as low volume resuscitants (LVRs). We found that RS-SBMA adversely affected coagulation in *in vitro* assays similar to PEG20K. We found that in a severe hemorrhagic shock model in rats, both RS-SBMA and RS-GmMA maintained MAP levels in the desired window for DCR and corrected hemorrhagic shock. Importantly, RS-GmMA did not show any significant impact on coagulation, which is vital to survival of trauma patients. We will continue to refine these therapies for prehospital care with DCR in future studies by directly measuring biodistribution, evaluating them in lethal models of hemorrhagic shock in combination with uncontrolled hemorrhage, and further optimizing potency of the therapeutic towards use in the prehospital setting.

Supporting Information

The authors have cited additional references within the Supporting Information. $\prescript{[39-58]}$

Acknowledgements

This work was supported by NIH NHLBI (1R01HL139007). TJP was supported by a National Science Foundation Graduate Research Fellowship under grant no. DGE-1762114. M.L. was also supported by a National Science Foundation Graduate Research Fellowship under grant no. DGE-214004. The authors acknowledge the use of facilities and instrumentation supported by the U.S. National Science Foundation through the Major Research Instrumentation (MRI) program (DMR-2116265) and the UW Molecular Engineering Materials Center (MEM-C), a Materials Research Science and Engineering Center (DMR-1719797). This work benefited from the use of the SasView

application, originally developed under NSF Award DMR - 0520547. SasView also contains code developed with funding from the EU Horizon 2020 programme under the SINE2020 project Grant No 654000. The authors would like to thank Brandon Bol and Martin Sadilek for their help with training for DSC measurements. The TA Discovery 2500 DSC instrument was funded by the University of Washington Student Technology Fee. The authors would like to thank Chang Yeop Han for his help with training for the thrombin generation assay.

Keywords: Hemorrhagic Shock • Low Volume Resuscitant (LVR) • RAFT Polymerization • Damage Control Resuscitation • Coagulation

- [1] C. J. Murray, A. D. Lopez, *The Lancet* **1997**, *349*, 1269–1276.
- [2] B. J. Eastridge, J. B. Holcomb, S. Shackelford, *Transfusion* 2019, 59, 1423–1428.
- [3] K. J. Kalkwarf, S. A. Drake, Y. Yang, C. Thetford, L. Myers, M. Brock, D. A. Wolf, D. Persse, C. E. Wade, J. B. Holcomb, Journal of Trauma and Acute Care Surgery 2020, 89, 716.
- [4] M. Revell, I. Greaves, K. Porter, *Journal of Trauma and Acute Care Surgery* **2003**, *54*, S63.
- [5] T. SHIRES, D. COLN, J. CARRICO, S. LIGHTFOOT, Archives of Surgery 1964, 88, 688–693.
- [6] M. Y. Zuidema, C. Zhang, World J Cardiol 2010, 2, 325–332.
- [7] R. L. Gruen, K. Brohi, M. Schreiber, Z. J. Balogh, V. Pitt, M. Narayan, R. V. Maier, *The Lancet* 2012, 380, 1099–1108.
- [8] J. B. Holcomb, D. Jenkins, P. Rhee, J. Johannigman, P. Mahoney, S. Mehta, E. D. Cox, M. J. Gehrke, G. J. Beilman, M. Schreiber, S. F. Flaherty, K. W. Grathwohl, P. C. Spinella, J. G. Perkins, A. C. Beekley, N. R. McMullin, M. S. Park, E. A. Gonzalez, C. E. Wade, M. A. Dubick, C. W. Schwab, F. A. Moore, H. R. Champion, D. B. Hoyt, J. R. Hess, *Journal of Trauma and Acute Care Surgery* 2007, 62, 307.
- [9] L. W. Chan, X. Wang, H. Wei, L. D. Pozzo, N. J. White, S. H. Pun, Sci. Transl. Med. 2015, 7, 277ra29-277ra29.
- [10] R. J. Lamm, E. B. Lim, K. M. Weigandt, L. D. Pozzo, N. J. White, S. H. Pun, *Biomaterials* 2017, 132, 96–104.
- [11] R. J. Lamm, T. J. Pichon, F. Huyan, X. Wang, A. N. Prossnitz, K. T. Manner, N. J. White, S. H. Pun, ACS Biomater. Sci. Eng. 2020, 6, 7011–7020.
- [12] T. J. Pichon, N. J. White, S. H. Pun, Current Opinion in Biomedical Engineering 2023, 27, 100456.
- [13] F. K. Butler, J. B. Holcomb, S. A. Shackelford, S. Barbabella, J. A. Bailey, J. B. Baker, A. P. Cap, C. C. Conklin, C. W. Cunningham, M. S. Davis, S. M. DeLellis, W. C. Dorlac, J. J. DuBose, B. J. Eastridge, A. D. Fisher, J. J. Glasser, J. M. Gurney, D. A. Jenkins, J. Johannigman, D. R. King, R. S. Kotwal, L. F. Littlejohn, R. L. Mabry, M. J. Martin, E. A. Miles, H. R. Montgomery, D. M. Northern, K. C. O'Connor, T. E. Rasmussen, J. C. Riesberg, P. C. Spinella, Z. Stockinger, G. Strandenes, D. K. Via, M. A. Weber, J Spec Oper Med 2018, 18, 37–55.
- [14] C. P. Boyan, Ann Surg 1964, 160, 282–286.
- [15] M. J. Mangino, L. K. Liebrecht, V. Plant, A. Limkemann, J. L. Pascual, J. W. Cannon, Hemorrhagic Shock: Recognition, Pathophysiology, and Management. Hauppauge, NY: Nova Publishers 2017.
- [16] M. Jungner, P.-O. Grände, G. Mattiasson, P. Bentzer, Anesthesiology 2010, 112, 1194–1203.
- [17] M. J. Delano, S. B. Rizoli, S. G. Rhind, J. Cuschieri, W. Junger, A. J. Baker, M. A. Dubick, D. B. Hoyt, E. M. Bulger, *Shock* 2015, 44, 25–31.
- [18] S. A. Stern, S. C. Dronen, P. Birrer, X. Wang, *Annals of Emergency Medicine* 1993, 22, 155–163.
- [19] D. S. Kauvar, R. Lefering, C. E. Wade, J Trauma 2006, 60, S3-11.

RESEARCH ARTICLE

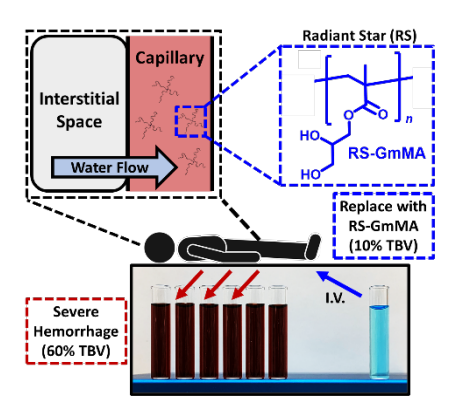
- [20] V. Plant, A. Limkemann, L. Liebrecht, C. Blocher, P. Ferrada, M. Aboutanos, M. J. Mangino, *J Trauma Acute Care Surg* 2016, 81, 1056–1062.
- [21] M. J. Mangino, *Polyethylene Glycol Polymers in Low Volume Resuscitation*, Virginia Commonwealth University, **2020**.
- [22] M. A. Bruusgaard-Mouritsen, B. M. Jensen, L. K. Poulsen, J. Duus Johansen, L. H. Garvey, *Journal of Allergy and Clinical Immunology* 2022, 149, 168-175.e4.
- [23] K. Wylon, S. Dölle, M. Worm, Allergy, Asthma & Clinical Immunology 2016, 12, 67.
- [24] J. Waniewski, M. Pietribiasi, L. Pstras, *Sci Rep* **2021**, *11*, 22150.
- [25] J. Wen, M. Weinhart, B. Lai, J. Kizhakkedathu, D. E. Brooks, Biomaterials 2016, 86, 42–55.
- [26] L. Almásy, O. P. Artykulnyi, V. I. Petrenko, O. I. Ivankov, L. A. Bulavin, M. Yan, V. M. Haramus, *Molecules* 2022, 27, 2573.
- [27] L. K. Liebrecht, J. Newton, E. J. Martin, N. Wickramaratne, S. Jayaraman, J. Han, M. Aboutanos, D. F. Brophy, M. J. Mangino, *PLOS ONE* 2018, 13, e0207147.
- [28] N. Wickramaratne, K. Kenning, H. Reichstetter, C. Blocher, R. Li, M. Aboutanos, M. J. Mangino, *Journal of Trauma and Acute Care Surgery* 2019, 87, 322–330.
- [29] J. G. Toffaletti, K. A. Buckner, Point of Care 2019, 18, 56.
- [30] L. Woodward, M. Alsabri, Cureus 2021, DOI 10.7759/cureus.16487.
- [31] R. Chapanian, I. Constantinescu, N. A. A. Rossi, N. Medvedev, D. E. Brooks, M. D. Scott, J. N. Kizhakkedathu, *Biomaterials* 2012, 33, 7871–7883.
- [32] M. Imran ul-haq, B. F. L. Lai, R. Chapanian, J. N. Kizhakkedathu, *Biomaterials* 2012, 33, 9135–9147.
- [33] M. Jawanda, B. F. L. Lai, J. N. Kizhakkedathu, K. Ishihara, R. Narain, *Polym. Chem.* 2013, 4, 3140–3146.
- [34] N. Nasongkla, B. Chen, N. Macaraeg, M. E. Fox, J. M. J. Fréchet, F. C. Szoka, J. Am. Chem. Soc. 2009, 131, 3842–3843.
- [35] D. Das, S. Srinivasan, F. D. Brown, F. Y. Su, A. L. Burrell, J. M. Kollman, A. Postma, D. M. Ratner, P. S. Stayton, A. J. Convertine, *Polym. Chem.* 2018, 9, 2134–2146.
- [36] D. Wilms, S.-E. Stiriba, H. Frey, Acc. Chem. Res. 2010, 43, 129–141.
- [37] A. S. Wolberg, R. A. Campbell, *Transfus Apher Sci* 2008, 38, 15–23.
- [38] E. E. Moore, H. B. Moore, L. Z. Kornblith, M. D. Neal, M. Hoffman, N. J. Mutch, H. Schöchl, B. J. Hunt, A. Sauaia, Nat Rev Dis Primers 2021, 7, 1–23.
- [39] M. Doucet, J. H. Cho, G. Alina, Z. Attala, J. Bakker, W. Bouwman, P. Butler, K. Campbell, T. Cooper-Benun, C. Durniak, L. Forster, M. Gonzalez, R. Heenan, A. Jackson, S. King, P. Kienzle, J. Krzywon, R. Murphy, T. Nielsen, L. O'Driscoll, W. Potrzebowski, S. Prescott, R. Ferraz Leal, P. Rozyczko, T. Snow, A. Washington, 2021, DOI 10.5281/zenodo.4467703.
- [40] P. Debye, J. Phys. Chem. 1947, 51, 18–32.
- [41] R.-J. Roe, Methods of X-Ray and Neutron Scattering in Polymer Science, Oxford University Press, Oxford, New York, 2000
- [42] H. Benoit, Journal of Polymer Science 1953, 11, 507-510.
- "star_polymer SasView 5.0.6 documentation," can be found under https://www.sasview.org/docs/user/models/star_polymer.html,
- [44] V. Plant, D. W. Parrish, A. Limkemann, P. Ferrada, M. Aboutanos, M. J. Mangino, J Pharmacol Exp Ther 2017, 361, 334–340.
- [45] T. K. Arora, A. K. Malhotra, R. Ivatury, M. J. Mangino, J Trauma Acute Care Surg 2012, 72, 397–402.
- [46] "7.1: Segment Models," can be found under https://chem.libretexts.org/Bookshelves/Biological_Chemistry/Concepts_in_Biophysical_Chemistry_(Tokmakoff)/02%3A_M acromolecules/07%3A_Statistical_Description_of_Macromolecular_Structure/7.01%3A_Segment_Models, 2021.

- [47] "Freely Jointed Chain," can be found under https://polymerdatabase.com/polymer%20physics/Kuhn.html, n d
- [48] "Persistence Length," can be found under https://polymerdatabase.com/polymer%20physics/lp%20Table. html, **n.d.**
- [49] "Characteristic Ratio," can be found under https://polymerdatabase.com/polymer%20physics/C%20Table2 %20.html, **n.d.**
- [50] S. Shiomoto, K. Inoue, H. Higuchi, S. Nishimura, H. Takaba, M. Tanaka, M. Kobayashi, *Biomacromolecules* 2022, 23, 2999–3008.
- [51] H. Yao, B. D. Olsen, Soft Matter 2021, 17, 5303-5318.
- [52] S. Mani, F. Khabaz, R. V. Godbole, R. C. Hedden, R. Khare, J. Phys. Chem. B 2015, 119, 15381–15393.
- [53] D. M. DiPerna, A. V. Prakapenka, E. P. Chung, R. W. Sirianni, in *Targeted Drug Delivery: Methods and Protocols* (Eds.: R.W. Sirianni, B. Behkam), Springer US, New York, NY, 2018, pp. 191–199.
- [54] C. Hall, E. Lueshen, A. Mošat', A. A. Linninger, Journal of Pharmaceutical Sciences 2012, 101, 1221–1241.
- [55] "Table A-10, Relative Liver Weights in Rats and Mice Following Inhalation Exposure for 28 Days (5 Days/Week, 6 Hours/Day)," can be found under https://www.ncbi.nlm.nih.gov/books/NBK601207/table/appa.ta b12/, 2023.
- [56] A. HEDIN, R. G. HAHN, Clinical Science 2005, 108, 217–224.
- [57] "Sprague Dawley® | Taconic Biosciences," can be found under https://www.taconic.com/products/mouse-rat/standard-strains-and-stocks/sprague-dawley#tabsmobiledropdown-46a3213b35-item-fae7f852c3-tab, n.d.
- [58] D. Parrish, V. Plant, S. L. Lindell, A. Limkemann, H. Reichstetter, M. Aboutanos, M. J. Mangino, *J Trauma Acute Care Surg* 2015, 79, 22–29.

WILEY -- VCH

RESEARCH ARTICLE

Entry for the Table of Contents



Traumatic injury is a leading cause of global suffering and death. We rationally design polymeric, low volume resuscitants (LVRs) for the prehospital treatment of severe hemorrhagic shock. By varying polymer architecture, R_g , and composition to influence resuscitation, coagulation, and biodistribution, we developed a radiant star polymer that is non-coagulopathic and corrects 60% total blood volume (TBV) loss when given at only 10% TBV. This highly portable LVR has profound potential for application in trauma medicine.